ELSEVIER

Earth and Planetary Science Letters 173 (1999) 333–342

EPSL

www.elsevier.com/locate/epsl

Laser shock experiments with nanoseconds pulses: a new tool for the reproduction of shock defects in olivine

F. Langenhorst [a,*], M. Boustie [b], A. Migault [b], J.P. Romain [b]

[a] *Bayerisches Geoinstitut, Universität Bayreuth, D-95440 Bayreuth, Germany*
[b] *Laboratoire de Combustion et de Détonique (UPR CNRS No. 9028), Ecole Nationale Supérieure de Mécanique et d'Aérotechnique, Site du Futuroscope, B.P. 109, F-86960 Futuroscope Cedex, France*

Received 31 March 1999; accepted 1 September 1999

Abstract

Laser shock experiments with olivine have been carried out in order to test the capability of this new experimental approach to produce known shock defects in olivine. To determine the shock conditions, numerical simulations of experiments have been undertaken, indicating the generation of a rapidly decaying shock wave with an initial pressure of 60 GPa and a duration of 5 ns. The pressure prevailed thus distinctly shorter than in conventional shock experiments with explosives or light gas guns (0.1–1 μs). Despite this shorter pressure pulse in our laser experiment, TEM revealed that a high density of dislocations and planar fractures was activated in olivine up to a depth of 30 μm. A drastic decrease of dislocation and fracture densities observed deeper in the sample is attributed to the decay of the shock wave. The dislocation systems and the orientations of planar fractures in our experiment are identical to those found in naturally shocked olivine. The TEM observations indicate furthermore that fractures in olivine are the sources of dislocations and that the stress field around fractures determines which slip system is activated. Our study demonstrates that laser shock experiments are not only a powerful new tool in the reproduction of shock defects but also an indispensable tool to understand better the role of time in impact processes and the formation mechanisms of shock defects.

Keywords: laser methods; shock metamorphism; planar deformation features; olivine

1. Introduction

Hypervelocity collisions are common processes in our solar system and played a major role in the formation of the planets, their satellites and the subsequent geological evolution of these bodies. The effects of such collisions range from the megascopic (formation of bowl-shaped or complex craters; cf. [1–3]) down to the submicroscopic scale (formation of shock defects in minerals; cf. [4–6]). On Earth, impact craters are often strongly eroded and, thus, the shock signature of minerals remains as the sole source of information on the impact event. The shock signature of minerals comprises a large variety of unique effects, such as the formation of one- to three-dimensional lattice defects, phase transformations, and decomposition [6]. These shock effects form in solid matter as result of the passage of dynamic compression (shock) waves that originate at the point of impact [7].

* Corresponding author. Tel.: +49 921 553727; Fax: +49 921 553769; E-mail: Falko.Langenhorst@uni-bayreuth.de

0012-821X/99/$ – see front matter
PII: S0012-821X(99)00224-1

Shock waves are commonly produced in experiments with high explosives or with light gas guns, which accelerate metal plates onto a target material [5,8,9]. In contrast to natural geological material, samples recovered from shock experiments are much faster quenched and do not experience post-shock hydrothermal alteration. Therefore, shock effects are generally preserved in their original state. Hence experiments are indispensable for a better understanding of the physical nature, formation mechanisms and natural post-shock modifications of shock effects [4,6,10–13]. Additionally, shock experiments performed under controlled conditions provide important calibration data on the occurrence of particular shock effects in certain pressure ranges [3,4].

The duration of the pressure pulse is an important experimental parameter, which can not be varied significantly with the conventional experimental designs. Therefore, our knowledge about the role of time in shock processes and the kinetics of shock-induced changes is very limited, and, so far, relies heavily on the comparison with natural geological material, which has been affected by longer pressure pulses (up to seconds) but also by strong post-shock annealing and alteration [13]. This comparison reveals, for example, that the pressure duration apparently exerts an important control on the rate of some phase transformations to high-pressure polymorphs and decomposition reactions, which have not been reproduced in experiments compared to nature or, if so only to a distinctly lesser extent [6,14]. On the other hand, shock-induced lattice defects in minerals have been duplicated to a large extent by conventional experiments. The lower time limits for the formation of these defects are largely unknown. A profound knowledge of the influence of time is however required to recognize specific effects that might be used as geospeedometer for impact events. A geospeedometer would be useful in constraining the sizes of the projectile and the resulting impact crater.

The use of short-pulse, high-energy lasers presents a new technique to generate shock waves with ultrashort (ns range) pressure pulses in geological materials. First attempts on quartz failed, however, to reproduce shock-induced lattice defects such as dislocations, planar fractures (PFs), and planar deformation features (PDFs, i.e., amorphous lamellae) [15], which probably reflects the need for longer pressure pulses to activate these defects in quartz. In a series of laser experiments on various rock-forming minerals with different experimental set-ups, we tried to duplicate natural shock defects [16]. Here we report on the first successful experiment on olivine, a major constituent of Earth's mantle and meteorites, which is known to deform more easily than quartz. The deformation features of the recovered sample were investigated by transmission electron microscopy, a method capable of analyzing very small sample volumes available. In addition, the laser experiment was simulated numerically in order to determine the pressure history and strain rate induced into the olivine target. The results of this study attest that laser shock experiments provide important information on the formation kinetics and formation mechanisms of shock-induced lattice defects.

2. Experimental and numerical techniques

Our high-pressure experiments have been carried out with a new experimental setup at the European Large Scale Facility LULI (Laboratoire pour l'Utilisation des Lasers Intenses, U.M.R. No. 7605 C.N.R.S./C.E.A./Ecole Polytechnique/Université Pierre et Marie Curie, 91128 Palaiseau Cédex, France), which is equipped with a high-power Neodymium- glass laser. The laser beam was directed and focused via mirrors and lenses onto the olivine sample, which was located in a furnace in the center of a vacuum chamber. Two Al foils were glued on the polished planar surface of the olivine sample and this arrangement was then clamped between two metal blocks (Fig. 1). The lower 0.5 mm thin Al foil with a 3 mm wide hole acted as spacing holder and was overlain by a 18 μm thin Al foil used as flyer plate. This flyer plate was driven by the ultra-short (2.5 ns) laser pulse and impacted the sample surface at high velocity. The shock front propagated parallel to the (001) plane of the olivine sample. This shock direction with respect to the crystal orientation is however only a first approximation because the shock front in small-scale laser experiments is not uniformly planar. For documentation, the chemical composition and lattice parameters of the olivine are given in Table 1. Prior to the experiment, the sample was heated in vacuum to

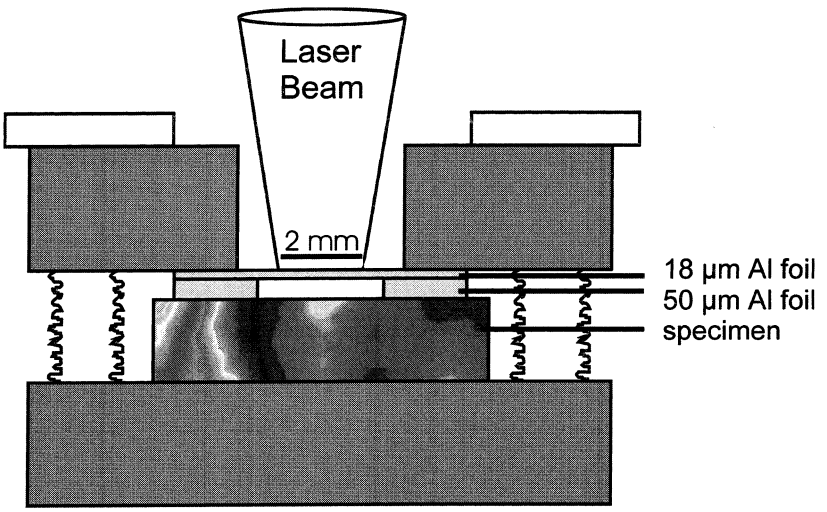

Fig. 1. Schematic drawing of the experimental set-up consisting of two Al foils and the olivine sample that is clamped between two metal blocks. This assembly was placed into the furnace so that the Al flyer faced the incident laser beam.

380ºC, the maximum temperature of the furnace, because easier deformation was expected to occur at this temperature. The recovered sample was subsequently investigated by optical microscopy (OM), scanning electron microscopy (SEM), and transmission electron microscopy (TEM). Thin sections cut perpendicular to the sample surface (cross-sections) were prepared to observe the shock damage as a function of depth. For TEM examination, these cross-sections were glued on copper grids and then thinned by argon ion beam bombardment. Determination of the Burgers vectors of dislocations was based on the $g \cdot b$ invisibility criterion. For imaging of dislocations the diffraction vector $g = [004]$ was mainly used.

Table 1
Normalized average composition of olivine sample determined by energy dispersive X-ray analysis (EDX) on a 200 kV analytical transmission electron microscope (ATEM) and lattice parameters a_o, b_o and c_o determined by X-ray powder diffractometry

	wt. %	Structural formula
Si	19.78	1.04
Ti	0.07	0.002
Fe	7.89	0.21
Ni	0.28	0.01
Mn	0.16	0.004
Cr	0.09	0.002
Mg	28.08	1.704
Ca	0.08	0.003
O	43.64	4.02
Fo		89.0
Fa		11.0
a (Å) 4.7525 ± 7		
b (Å) 10.2116 ± 18		
c (Å) 5.9806 ± 11		

Since present experimental techniques are almost incapable of measuring accurately the physical conditions prevailing in these miniature shock experiments, the shock parameters induced in the olivine sample by the laser-driven flyer have been estimated with two numerical codes. The FILM code developed at LULI computes the laser interaction with matter [17]. The laser lightening conditions on the aluminium flyer (energy pulse shape, intensity on the aluminium surface, laser wavelength etc.) control the corresponding pressure profile induced on the front face of the aluminium (Fig. 2). In our experiment, laser beam diameter, pulse, and energy were 2 mm, 2.5 ns, and 77.1 J, respectively, leading to an intensity of 982 GW/cm^2 on the aluminium flyer. These input parameters for the FILM code result in a peak pressure pulse of 26.5 GPa applied to the aluminium [18]. The pressure profile induced in the aluminium flyer is then used as input condition for simulating its propagation with the code SHYLAC [19]. This 1D Lagrangian code written in finite differences solves the conservative equations in hydrodynamic media with a Mie–Grüneisen equation of state ref-

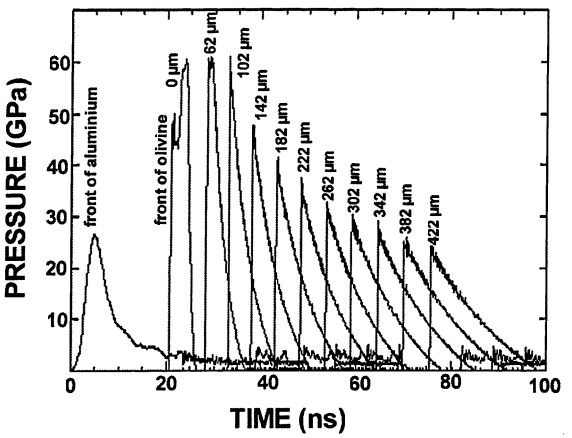

Fig. 2. Initial pressure pulse applied to the 18 µm flyer plate and resulting pressure profiles at different depths in the olivine. The origin of the abscissa has been chosen to be on the impacted olivine face that was separated by a 50 µm hole from the back surface of the aluminium flyer.

erenced to the Hugoniot using a linear relationship between the shock speed D and the particle velocity u ($D = C_o + su$ where C_o is the sound velocity and s the slope); the parameters used in the simulation are listed in Table 2 [20–23]. The pressures and pulse durations were determined directly from the shock wave profiles calculated for different penetration depths by the code SHYLAC. The strain rates $\dot{\varepsilon}$ generated on every part of the target have been calculated from the positions $x(i, n)$ of the cell i at time $t(n)$ and their particle velocity $u(i, n)$:

$$\dot{\varepsilon}(i, n) = \frac{u(i, n) - u(i-1, n)}{x(i, n) - x(i-1, n)}$$

In order to monitor the change of strain rates $\dot{\varepsilon}$ as a function of propagation time of the shock wave, we have determined the maximum value of $\dot{\varepsilon}$ on every cell i at various times $t(n)$.

Table 2
The input parameters density ρ, sound velocity C_o, and the slope s of the linear relationship between the shock speed and the particle velocity used for numerical simulation [20–23]

	ρ (g/cm^3)	C_o (m/s)	s
Olivine	3.3	5.87	1.25
Aluminium	2.715	5.386	1.339

3. Results

3.1. Numerical data

The data determined by the numerical simulation of the laser experiment are depicted in Figs. 2 and 3. The initial pressure profile induced in olivine has a maximum amplitude of about 60 GPa with an average duration of 5 ns (Fig. 2). Compared to direct irradiation of the sample, the use of our laser-driven foil technique leads to an increase in both the amplitude and the duration of the pressure pulse by a factor of 2. The pressure profile induced into the olivine sample features roughly a two-step shape. The first step is generated by the impact of the flyer and the second one is due to reloading as the shock waves go back and forth into the flyer after the impact. The calculated pressures at various depths from the impacted surface of the olivine are shown in Fig. 3a. Pressure remains constant up to a depth

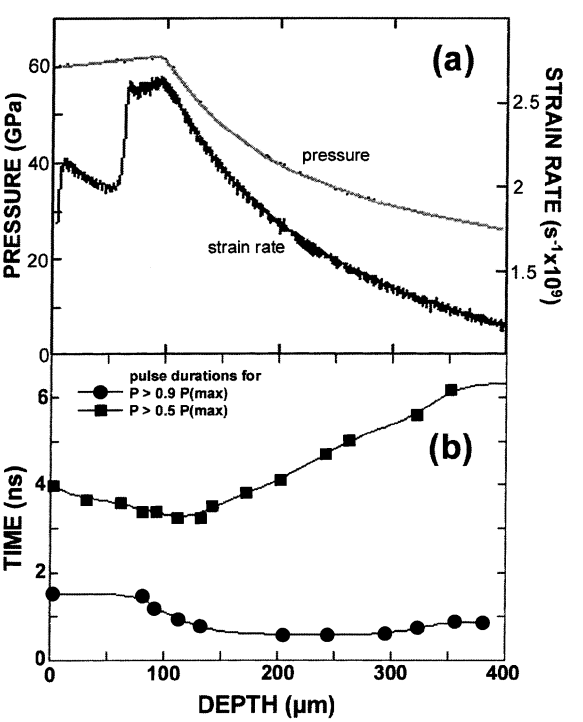

Fig. 3. (a) Evolution of pressure and maximum values of the strain rate as a function of the depth in olivine, and (b) length of time when pressure was greater than 50% and 90% of peak pressure versus depth in olivine.

of 100 μm and then decays. This decay is due to the release wave of the loading, which overtakes the transmitted shock wave.

The evolution of the strain rate is in line with the evolution of the pressure profile induced by the collision (Fig. 3a): the first step in strain rates is due to the impact of the flyer, which yields a strain rate of about 2.0×10^9 s^{-1}. This strain rate is maintained during the time of a back and forth of the wave into the 18 μm thick aluminium flyer, leading to a reloading of olivine with a rise of the strain rate up to 2.6×10^9 s^{-1}. At a depth of >100 μm, the strain rate decreases then because of the decay of the shock wave.

The pulse duration in laser experiments is difficult to define because the pulse shape is ideally gaussian and a clear pressure plateau is absent ([18], Figs. 2 and 3b). Therefore, we have calculated the length of time (pulse duration) when the pressure was greater than 50% and 90% of the maximum peak height. The 90% duration of the peak pressure remains almost constant over the first 100 μm and then also decreases when the decay of the shock begins. For the 50% duration of the maximum pressure, we observe first a slight decay followed by an increase due to the spreading of the fan of release waves.

3.2. Optical and TEM observations

Inspection of the shocked olivine sample with OM and SEM revealed an intact surface (Fig. 4), i.e., due to the sandwich configuration, ejection of sample material was prevented. By contrast, the formation of a crater and ejection of material was observed in previous laser experiments on quartz with direct irradiation [15]. Optical examination of olivine cross-sections under crossed Nicols showed a mottled extinction pattern, which, in shock nomenclature, is referred to as mosaicism [12]. Pervasive fracturing of the olivine occurs up to a depth of 150 μm. This optical observation indicated that subsequent TEM analysis should concentrate on the uppermost part of the sample.

Microstructural TEM investigation in the vicinity of the point of impact shows that the olivine sample contains two distinct shock defects (Figs. 5 and 6): (1) a large number of planar and irregular fractures, and (2) numerous dislocations.

Planar fractures (PFs) are clearly more abundant than irregular ones. The two sides of PFs are generally in close contact with each other, whereas irregular fractures occur in most cases as open cracks.

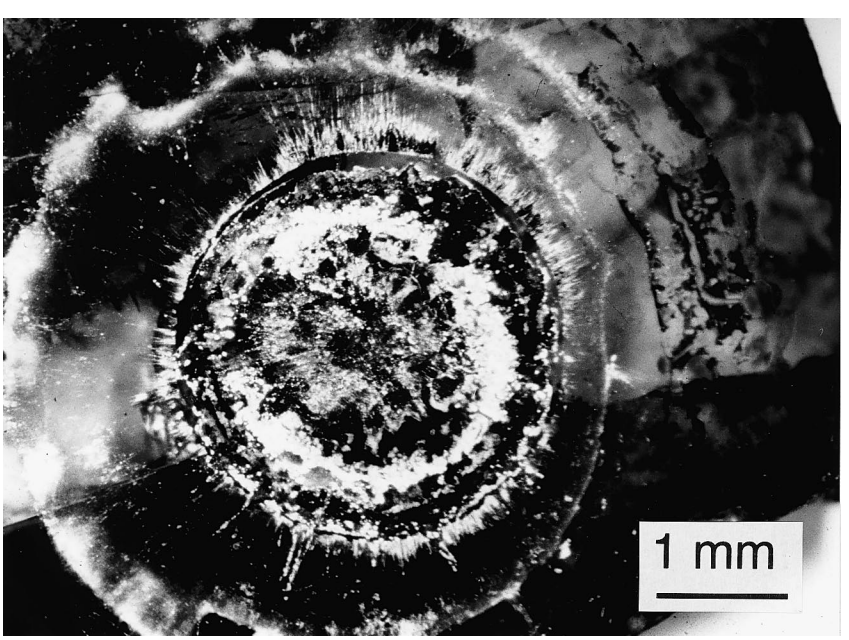

Fig. 4. Optical micrograph of the impacted olivine surface in reflected light. The olivine surface is partially covered by the circular remnants of the Al flyer plate.

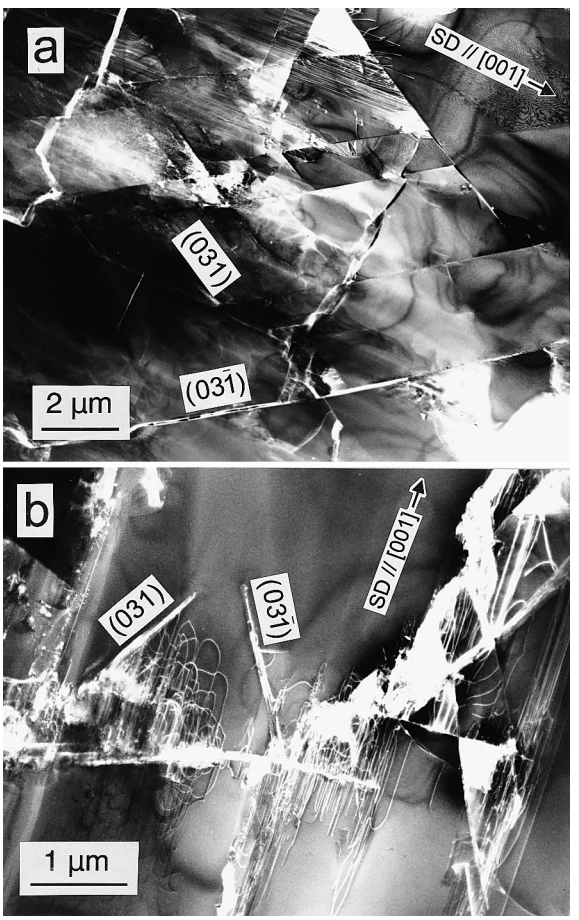

Fig. 5. Weak beam TEM images of planar fractures in the shocked olivine; diffraction vector $g = [004]$; *SD* = shock direction. Note in (a) that one set of fractures is terminated by a second intersecting set of fractures. In (b), the planar fractures (031) and (03$\bar{1}$) are arrested inside of the crystal.

Most PFs do not penetrate the entire olivine crystal. They are often terminated by intersections with other crossing PFs or are arrested within the crystal (Fig. 5). On the basis of selected area electron diffraction (SAED) patterns, the orientations of PFs were identified. According to decreasing abundance, PFs occur parallel to the following planes: (031), (03$\bar{1}$), (023), (0$\bar{2}$3), (041), (04$\bar{1}$), and very subordinate (100) and (001). The most abundant PFs are dense planes in the olivine structure, which have inclinations to the (001) surface plane of olivine of 67° (041), 60° (031), and 21° (023). These planes do not coincide with the direction of maximum resolved shear stress, which is at 45° to the surface. This demonstrates that the crystal structure exerts an important control on the orientation of planar fracturing. The PF planes activated are the densest crystallographic planes available close to the direction of maximum resolved shear stress. In general, PF orientations match perfectly those known for olivine shocked in nature or conventional shock [10,24–26]. It is important to note that, in contrast to PFs, irregular fractures often occur either approximately parallel or perpendicular to the shock front. Altogether, the number of planar and irregular fractures per μm^{-2} varies with depth d. A considerable decrease of the number of fractures is recognizable at $d > 30$ μm, reaching a minimum at $d > 100$ μm (Fig. 7a).

Dislocations are generally associated with fractures as dislocations originate at fractures and are highly concentrated around them (Fig. 5b and Fig. 6b). Dark-field TEM imaging reveals the invisibility of dislocations when using diffraction vectors perpendicular to [001], which, in turn, indicates that the Burgers vectors are exclusively [001]. As can be recognized at arrested fractures, the [001] Burgers vector is always perpendicular to the line marking the end of an arrested fracture. Dislocations with Burgers vector [001] are principally known to dominate over dislocations with the shorter [100] Burgers vector if high strain rates are applied at relatively low (<800°C) temperatures [27–30]. The [001] dislocations occur as elongated loops and have thus both screw and, at the end, edge segments (Fig. 6c). Screw segments are distinctly longer than edge segments, suggesting the higher mobility of the edge component. The presence of edge segments enabled the determination of the slip planes (010), (100), and those belonging to the form {110}. At the inclined PFs, the [001](010) and, to a lesser extent, the [001]{110} slip systems clearly dominate over the [001](100) slip system. At irregular fractures, all three slip systems seem to be equally activated. These slip systems are also typically found in olivine shocked in nature or conventional shock experiments [26,31–33]. If dislocations are emitted in different slip planes at a fracture, interaction occurs between the slip systems forming a network of dislocations (Fig. 6d). The edge segments of dislocations are elastically distorted when they cross the screw segments

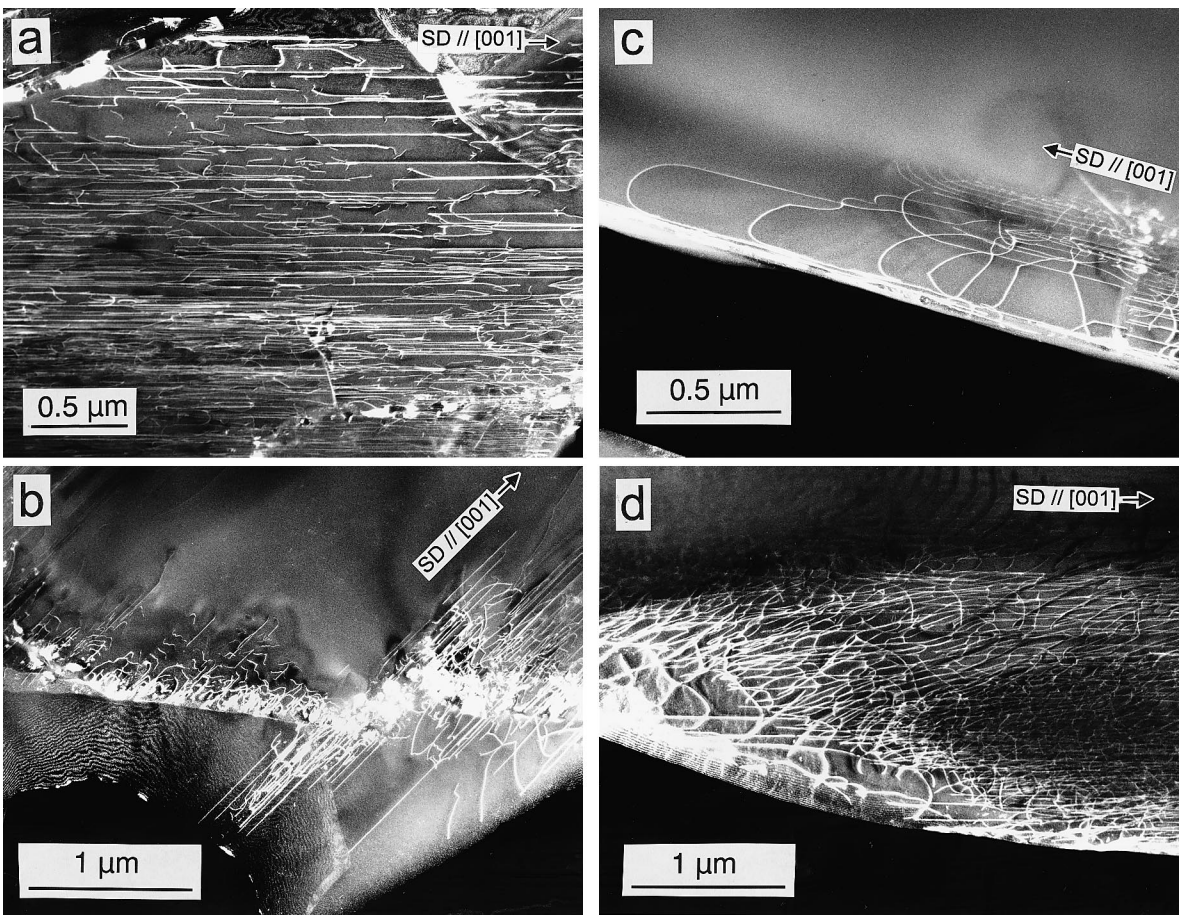

Fig. 6. Weak beam TEM images of [001] dislocations in the shocked olivine; diffraction vector $g = [004]$, *SD* = shock direction. (a) Region with very high dislocation density of approximately 10^{14} m^{-2}. (b) [001] dislocations emitted from a planar fracture. (c) Elongated dislocation loops with the screw component being longest segment. (d) A three-dimensional network of [001] dislocations activated in different slip planes.

of adjacent dislocations, demonstrating the repulsive forces active between crossing dislocation systems.

The dislocation density shows a similar tendency as the fracture density, i.e., an enormous decrease at a depth $d > 30$ μm (Fig. 7b). Highest dislocation densities of up to 1.4×10^{14} m^{-2} occur below this depth (Fig. 6a). Similar dislocation densities have also been measured in naturally shocked olivine [26,32]. The dislocation density in our sample is heterogeneously distributed. Wherever there are fractures, the dislocations are always highly concentrated but the number of fractures and, hence, the amount of defect-free area increases with increasing depth. This results in the observed decrease of dislocation density as function of depth. Due to the numerous dislocations the internal energy of the olivine is enhanced. Given the highest dislocation density of 1.4×10^{14} m^{-2} we calculated the self energy of screw dislocations [29] and found that an elastic energy of approximately 1.4 J/cm^3 is stored in the olivine. Such high elastic energies may be important in the phase transformation of olivine to its higher-pressure polymorphs that due to the longer pressure pulse occurs in nature.

On the basis of the length of dislocation lines (maximum distance to fracture), the calculated pulse, and under consideration of the propagation direction of the shock wave it was possible to estimate the dislocation velocity. The longest dislocation lines are observed on the side of fractures where sliding in the direction of shock is possible. On the other sides, dis-

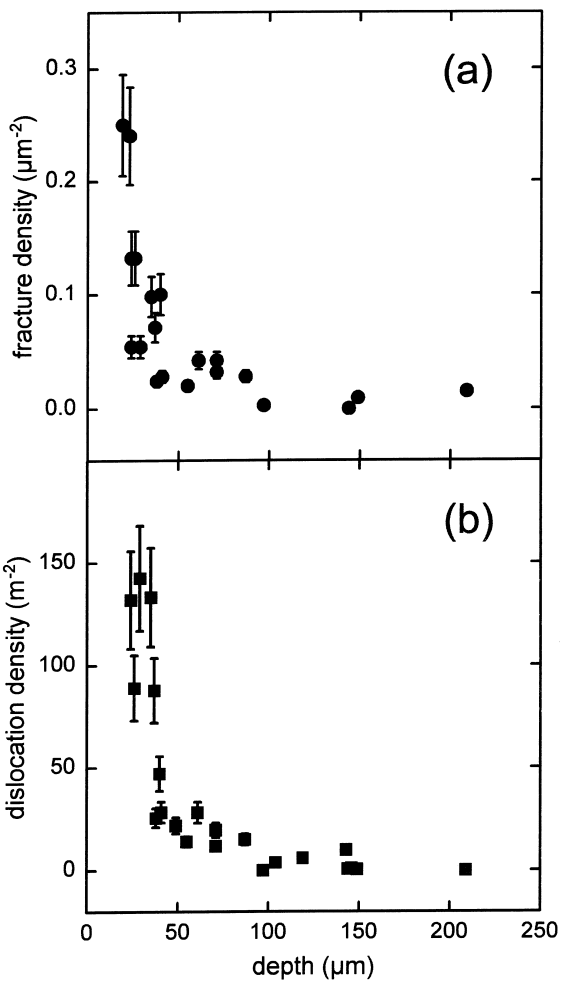

Fig. 7. (a) Fracture and (b) dislocation densities as function of depth in the shocked olivine.

locations are shorter because they moved opposite to the shock front and had, thus, less time for propagation. Calculations result in dislocation velocities of up to 2 km/s, which is about 1/3 of the sound velocity in olivine, the theoretical upper limit of dislocation velocity. Most dislocations seem, however, to have migrated with velocities of approximately 1 km/s. It is important to note that these velocities are minimum estimates of velocities as it is unknown whether or not the dislocations formed during the pressure rise and propagated subsequently over the total time span of the shock pulse. Additionally, it should be considered that the longest dislocation segments are often terminated by neighbouring fractures.

4. Discussion

To our knowledge, we demonstrate for the first time that ultra-short laser experiments are suitable for the production of the microstructural shock defects that occur in naturally shocked minerals. Mosaicism, planar fractures, and dislocations with Burgers vector [001] observed in our olivine sample occur to a similar extent in natural samples [12,26,32]. These results indicate that the formation of shock defects in olivine is almost instantaneous. In principle, experimental data on the occurrence of the shock defects in specific pressure ranges should thus be applicable to derive the shock conditions of naturally shocked olivine.

The observed decrease in fracture and dislocation densities at 30 to 50 μm depth is related to the decay of the shock wave (Fig. 7). The numerically calculated pressure and strain rate attenuations start, however, at a depth of about 100 μm and seem to be too long (Fig. 3). This obvious discrepancy between observation and calculation is probably due to the ideal assumptions in the simulation. Assumptions such as the absolute planarity of the shock front and the absence of ablation of the aluminum target are certainly not fulfilled in the shock experiment. Additionally, it has to be taken into account that the simulation is performed for 1D propagation, assuming no 2D attenuation from the spatial unloading.

The results of our study also shed light on the formation kinetics and formation mechanisms of shock defects in olivine. Despite the high dislocation velocity of up to 2 km/s, the ultra-short laser pulse prevented the entire pervasion of olivine by dislocations. The shock speed was higher than the dislocation velocity because dislocation mobility was probably hampered by the interaction of different slip systems and the formation of a three-dimensional dislocation network. In metallurgy, this process is well known as work hardening. In addition, during propagation the dislocations were overtaken by the rarefaction wave, which immediately stopped the slip process. The observation that dislocation lines are, in most cases, longer on the side of fractures that face into the shock direction supports this interpretation. In conclusion, the dislocation density and its decrease with depth are not only controlled by the pressure but also by the pulse duration. This influence of time

should not be recorded in nature because natural shock events last 7 to 9 orders of magnitude longer than the ultra-short laser pulses, i.e., due to sufficient pulse duration and the high dislocation velocity, dislocations totally pervade naturally shocked olivine. It is thus not possible to use the dislocation density or the length of dislocations in olivine for estimating the shock duration in nature.

The overall correlation between fracture and dislocation densities and the general occurrence and high concentration of dislocations at fractures indicate that dislocations nucleate at fractures. There are several ways of envisaging the role of fractures in the formation of dislocations. Within the short time frame given by the laser experiment, the fractures could be considered as the only available sites for the nucleation of dislocations under the overall high shock stresses. Alternatively, dislocations could form at fractures due to stress concentration at the tips of developing fractures. This latter approach is similar to the classical theory of dislocation formation at fractures in materials deformed at ambient pressures [34–36]. As described below, this theory can provide insight into the mode of fracturing and also explains the preferential activation of certain slip systems.

TEM studies on brittle solids have shown that dislocations can be activated at the tips of fractures by three modes of deformation [34–36]: the opening (I), sliding (II), and tearing modes (III). In case of the opening and sliding modes, dislocations with Burgers vectors perpendicular to the fracture line (line marking the end of an arrested fracture) are observed, whereas the tearing mode leads to the formation of dislocations with Burgers vectors parallel to the fracture line. In our sample, dislocations belong to the first category, i.e., they have been formed by the opening and/or sliding modes. PFs occur mainly as closed fractures, suggesting formation by the sliding mode during the compression phase. On the other hand, irregular fractures are often open, which would favour the opening mode during the decompression phase. Their formation could be explained as a spallation effect. The general observation that PFs continue when they cross open irregular fractures supports the idea that PFs are formed earlier than the irregular fractures.

The characterization of dislocations in the olivine indicates furthermore that the stress field at the tips of fractures determines which slip system is activated. Assuming that a shock wave produces a uniaxial stress in the shock direction it has to be expected that, according to the Schmid law [37], the maximum resolved shear stress is at 45° to the shock direction, which propagated in our experiment parallel to the *c*-axis of olivine. However, all glide planes active in the olivine are parallel to the *c*-axis, where practically no shear stress should be present. This demonstrates that the local stress field around the opening fractures is likely the controlling factor for the activation of the glide systems. Assuming that the stress is locally active along the fractures, the Schmid factors S ($S = \cos\psi \cos\lambda$ where ψ and λ are the angles between the direction of load and the normal to the slip plane and the slip direction, respectively) for the observed glide planes can be calculated. For example, at the observed planar fractures parallel to (031) the Schmid factors S for the (010) and {110} planes are on the order of 0.5, whereas $S = 0$ for the glide plane (100). This plausibly explains why the (010) and {110} planes clearly dominate over the (100) glide plane.

Acknowledgements

The access to LULI facilities has been supported by the European Commission under the Access to Large-Scale Facility Activity of the Training and Mobility of Researchers Program within the TMR Large Scale Facility contract No. FMGE CT950044. Further financial support was povided by a PROCOPE programme to A. Deutsch and U. Schärer. We thank P. Agrinier for contributions to the performance of the experiment, S. Mackwell for careful corrections on the manuscript, and P. Cordier and A. El Goresy for constructive reviews. ***[FA]***

References

[1] R.A.F. Grieve, Terrestrial impact structures, Annu. Rev. Earth Planet. Sci. 15 (1987) 245–270.
[2] H.J. Melosh, Impact Cratering — A Geologic Process, Oxford University Press, New York, 1989, 245 pp.
[3] A. Deutsch, F. Langenhorst, Mineralogy of astroblemes — terrestrial impact craters: introduction, cratering and shock metamorphism, characteristics of terrestrial impact struc-

tures, geological formations in and around impact structures, in: A.S. Marfunin (Ed.), Advanced Mineralogy — Mineral Matter in Space, Mantle, Ocean Floor, Biosphere, Environmental Management, and Jewelry, Springer, Berlin, 1998, Vol. 3, pp. 76–95 and 132–139.
[4] D. Stöffler, Deformation and transformation of rock-forming minerals by natural and experimental shock processes, I: Behaviour of minerals under shock compression, Fortschr. Mineral. 49 (1972) 50–113.
[5] D. Stöffler, F. Langenhorst, Shock metamorphism of quartz in nature and experiment, I: Basic observation and theory, Meteoritics 29 (1994) 155–181.
[6] F. Langenhorst, A. Deutsch, Mineralogy of astroblemes — terrestrial impact craters: minerals in terrestrial impact structures and their characteristic features, in: A.S. Marfunin (Ed.), Advanced Mineralogy — Mineral Matter in Space, Mantle, Ocean Floor, Biosphere, Environmental Management, and Jewelry, Springer, Berlin, 1998, Vol. 3, pp. 95–119 and 132–139, .
[7] M.B. Boslough, J.R. Asay, Basic principles of shock compression, in: J.R. Asay, M. Shahinpoor (Eds.), High-Pressure Shock Compression of Solids, Springer, New York, 1993, pp. 7–42.
[8] J.R. Asay, M. Shahinpoor, High-Pressure Shock Compression of Solids, Springer, New York, 1993, 393 pp.
[9] I.M. Barker, M. Shahinpoor, L.C. Chhabildas, Experimental and diagnostic techniques, in: J.R. Asay, M. Shahinpoor (Eds.), High-Pressure Shock Compression of Solids, Springer, New York, 1993, pp. 43–73.
[10] W.U. Reimold, D. Stöffler, Experimental shock metamorphism of dunite, Proc. Lunar Planet. Sci. Conf. 9 (1978) 2805–2824.
[11] J.F. Bauer, Experimental shock metamorphism of mono- and polycrystalline olivine: a comparative study, Proc. Lunar Planet. Sci. Conf. 10 (1979) 2573–2596.
[12] D. Stöffler, K. Keil, R.D. Scott, Shock metamorphism of ordinary chondrites, Geochim. Cosmochim. Acta 55 (1991) 3845–3867.
[13] R.A.F. Grieve, F. Langenhorst, D. Stöffler, Shock metamorphism of quartz in nature and experiment, II: Significance in geoscience, Meteoritics 31 (1996) 6–35.
[14] F. Langenhorst, Shock experiments on α- and β-quartz, II: X-ray and TEM investigations, Earth Planet. Sci. Lett. 128 (1994) 683–698.
[15] P. Cordier, J.C. Doukhan, A. Migault, J.P. Romain, Microstructural investigation of quartz submitted to ultra-short shock loading, J. Mater. Sci. 30 (1995) 4009–4013.
[16] F. Langenhorst, M. Boustie, U. Schärer, D. Stöffler, Laser shock experiments on rock-forming silicates: a TEM examination, Lunar Planet. Sci. Conf. XXVII, 1996
[17] S. Atzeni, The physical basis for numerical fluid simulations in laser fusion, Plasma Phys. Controlled Fusion 29 (1987) 11.
[18] S. Couturier, T. de Resseguier, M. Hallouin, J.P. Romain, F. Bauer, Shock profile induced by short laser pulses, J. Appl. Phys. 79 (12) (1996) 9338–9342.
[19] F. Cottet, M. Boustie, Spallation studies in aluminum targets using shock waves induced by laser irradiation at various pulse durations, J. Appl. Phys. 66 (1989) 4067.
[20] I. Jackson, T.J. Ahrens, Shock wave compression of single-crystal forsterite, J. Geophys. Res. 84 (1979) 3039–3048.
[21] R. Jeanloz, Shock effects in olivine and implications for Hugoniot data, J. Geophys. Res. 85 (1980) 3163–3176.
[22] S.P. Marsh, LASL Shock Hugoniot Data, University of California Press, Berkeley, CA, 1980, 685 pp.
[23] Y. Syono, T. Goto, J.-I. Sato, H. Takei, Shock compression measurements of single-crystal forsterite in the pressure range 15–93 GPa, J. Geophys. Res. 86 (1981) 6181–6186.
[24] W.F. Müller, U. Hornemann, Shock-induced planar deformation structures in experimentally shock-loaded olivines and in olivines from chondritic meteorites, Earth Planet. Sci. Lett. 7 (1969) 251–264.
[25] L.W. Snee, T.J. Ahrens, Shock-induced deformation features in terrestrial peridot and lunar dunite, Proc. Lunar Sci. Conf. 6 (1975) 833–842.
[26] F. Langenhorst, P. Joreau, J.C. Doukhan, Thermal and shock metamorphism of the Tenham meteorite: a TEM examination, Geochim. Cosmochim. Acta 59 (1995) 1835–1845.
[27] N.L. Carter, H.G. Avé Lallemant, High temperature flow of dunite and peridotite, Geol. Soc. Am. Bull. 81 (1970) 2181–2202.
[28] J.P. Poirier, On the slip systems of olivine, J. Geophys. Res. 80 (1975) 4059–4061.
[29] A. Nicolas, J.P. Poirier, Crystalline Plasticity and Solid State Flow in Metamorphic Rocks, Wiley, New York, NY, 1976, 444 pp.
[30] A.C. McLaren, Transmission Electron Microscopy of Minerals and Rocks, Cambridge University Press, Cambridge, 1991, 387 pp.
[31] J.R. Ashworth, D.J. Barber, Electron petrography of shock-deformed olivine in stony meteorites, Earth Planet. Sci. Lett. 27 (1975) 43–50.
[32] M. Madon, J.P. Poirier, Transmission electron microscope observation of α, ß and γ $(Mg,Fe)_2SiO_4$ in shocked meteorites: planar defects and polymorphic transitions, Phys. Earth Planet. Inter. 33 (1983) 31–44.
[33] F. Langenhorst, R.T. Schmitt, J.C. Doukhan, Shock experiments with H6 chondrite Kernouvé, III: A TEM characterization of shock defects, Third International Workshop of the Scientific Network of the European Science Foundation, Limoges, Collection of Abstracts, 43, 1994.
[34] B.R. Lawn, B.J. Hockey, S.M. Wiederhorn, Atomically sharp cracks in brittle solids: an electron microscopy study, J. Mater. Sci. 15 (1980) 1207–1223.
[35] S.M. Ohr, An electron microscope study of crack tip deformation and ist impact on the dislocation theory of fracture, Mater. Sci. Eng. 72 (1985) 1–35.
[36] R.M. Thomson, Physics of fracture, J. Phys. Chem. Solids 48 (11) (1987) 965–983.
[37] E. Schmid, W. Boas, Plasticity of Crystals, F.A. Hughes, London, 1950.